

# DEPTHFORMER: MULTIMODAL POSITIONAL ENCODINGS AND CROSS-INPUT ATTENTION FOR TRANSFORMER-BASED SEGMENTATION NETWORKS

Francesco Barbato, Giulia Rizzoli, Pietro Zanuttigh

Department of Information Engineering  
University of Padova  
Via Gradenigo 6/a, Padova, Italy

## ABSTRACT

Most approaches for semantic segmentation use only information from color cameras to parse the scenes, yet recent advancements show that using depth data allows to further improve performances. In this work, we focus on transformer-based deep learning architectures, that have achieved state-of-the-art performances on the segmentation task, and we propose to employ depth information by embedding it in the positional encoding. Effectively, we extend the network to multimodal data without adding any parameters and in a natural way that makes use of the strength of transformers’ self-attention modules. We also investigate the idea of performing cross-modality operations inside the attention module, swapping the key inputs between the depth and color branches. Our approach consistently improves performances on the Cityscapes benchmark.

*Index Terms*— Semantic Segmentation, Sensor Fusion, Vision Transformers, Positional Encoding, Cross Attention

## 1. INTRODUCTION

Semantic Segmentation, i.e., pixel-wise classification of an input image, has recently become a very active research field, especially given the potential applications in Autonomous Driving. Among approaches for this task, architectures based on convolutional models have achieved-state-of-the-art results for many years [1]. More recently, after being adapted to vision tasks in the ViT work [2], transformer-based approaches [3] have started to come up. SegFormer [4], the architecture on which our work is based on, is an example of this class. Furthermore, recent research has also shown that multimodal approaches, exploiting also depth or other side information, allow to further improve performances [5].

In this paper, we propose to tackle multimodal semantic segmentation with two different strategies tailored for transformer-based architectures. Firstly, we

design a way to inject depth information in the positional encoding of a transformer, effectively expanding the embedding latent dimensionality from 2D to 3D, with a noticeable gain in the final segmentation accuracy and with no additional parameters or significant computational cost. Secondly, we consider the three inputs of a transformer self-attention head, and propose to swap such inputs between parallel architectures fed with different modality inputs. We report results supporting our design choices.

The article is structured as follows: in Sec. 2 we report a survey of the related works; then, a detailed description of our approach is presented in Sec. 3; Sec. 4 contains the numerical results and ablation studies on the Cityscapes [6] dataset; finally, in Sec. 5 we provide conclusive remarks and possible future perspectives. We also provide the source code of our approach<sup>1</sup>.

## 2. RELATED WORKS

After showing impressive results in text recognition, attention-based strategies attempting to capture long-range relationships between input data have recently been applied to vision tasks. The Vision Transformers (ViT) [2] work introduced a convolution-free vision strategy based on transformers capable of outperforming prior state-of-the-art methods in image classification. SegFormer [4] is a variation of the model tackling semantic segmentation. It contains a positional-encoding-free, hierarchical Transformer encoder and a lightweight all-MLP decoder.

Recent research has shown that other modalities such as depth and thermal cameras can support the extraction of semantic cues [5, 7, 8, 9]. The first attempts at multimodal semantic segmentation combine RGB data with other modalities into multi-channel representations, which are subsequently fed into traditional semantic segmentation networks built on the encoder-decoder framework [10, 11]. This straight-

<sup>1</sup>This work has been in part supported by the University of Padova under the project "SID2020 Semantic Segmentation in the Wild".

<sup>1</sup>The source code will be made available upon publication.

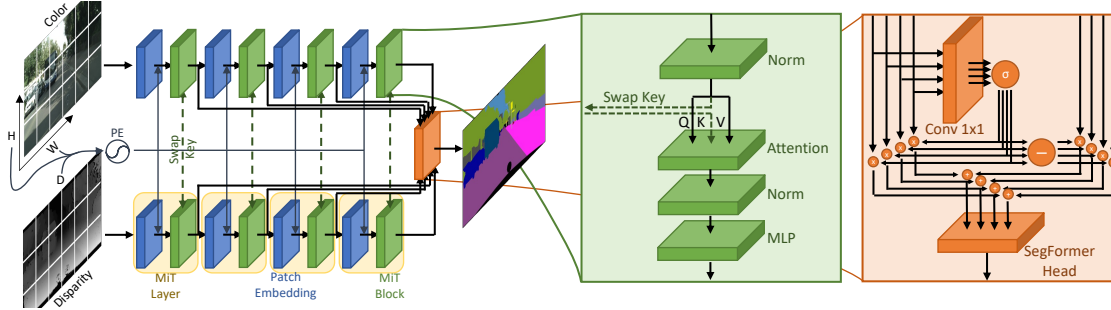


**Fig. 1:** Graphical representation of our architecture, we highlight the Cross-Input Attention (CIA, in green) and the Attention-Mix (AM, in orange) modules. Note that the two encoder branches share weights.

forward early fusion strategy struggles to capture the different types of information carried by the various modalities and, as a result, it is not very effective. The majority of current methods attempt to combine the early, feature, and late-fusion strategies in the best possible way by performing several fusion operations at various levels in the deep network [7, 12, 13]. A popular architectural choice is using a multi-stream encoder with a network branch processing each modality together with additional network modules connecting the different branches that combine modality-specific features into fused ones and/or carry information across the branches [7, 8, 14]. This hierarchical fusion technique creates a more precise feature map by utilizing multilevel features through incremental feature merging. Instead of only at early or late stages, this approach requires to fuse information at multiple levels. Multilevel features can be supplied in this way either mutually between modalities [7, 8] or in one-way, as in [15], where depth cues are sent to the RGB branch.

### 3. PROPOSED METHOD

In this section, we present a detailed description of our approach (see Fig. 1), starting from introducing the employed framework and then detailing the proposed 3D Positional Encoding (PE) and cross-attention strategies. Our approach moves from the recent and well-performing SegFormer [4] architecture, whose backbone has been modified to make use of Positional Encodings instead of the Mix-FFN layer. The PE is injected before each processing block, similarly to the Pyramid Vision Transformer [16] backbone. To account for the multimodal input, we adapted the SegFormer architecture in a dual-stream version, where the depth information (represented through disparity data) is forwarded to the Positional Encoding and to one of the two branches as well. Compared to previous research we introduce two key achievements, a novel positional encoding scheme (Sec. 3.1) and a multi-modal attention scheme (Sec. 3.2).

#### 3.1. 3D Positional Encoding

The starting point for the design of our positional encoding is the scheme presented in [3], which encodes the position of a token in a sequence using a multidimensional function  $\vec{PE}: \mathbb{R} \mapsto \mathbb{R}^C$ . We chose this type of encoding, rather than a learned one because it accepts arbitrary 1-dimensional inputs and can be used to embed the depth information. More in detail, we used the following encoding function:

$$\vec{PE}(i)[c] = \begin{cases} \sin(i\pi 2^{\log_2 I} c/C) & \text{if } c \bmod 2 = 0 \\ \cos(i\pi 2^{\log_2 I} c/C) & \text{if } c \bmod 2 = 1 \end{cases} \quad (1)$$

where the position  $i$  is normalized in the range  $[0, 1]$ ,  $I$  is the maximum value of  $i$  before normalization and  $C$  is the number of dimensions (note that  $c$  is 0-indexed). Notice that in [3] the frequencies used in the embedding reach up to  $10^5$ , to account for long input sequences in natural language processing. In our case, the sequence length is the image side (i.e., 512px) therefore we change the scaling factor accordingly. See Fig. 2 for a graphical representation of the resulting encoding.

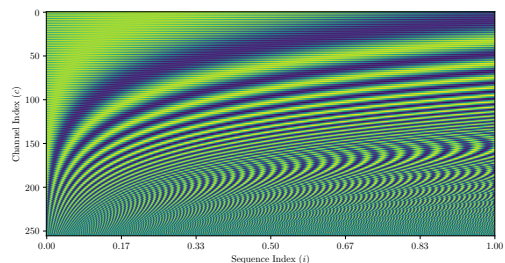


**Fig. 2:** Graphical representation of the  $\vec{PE}$  embeddings.

To handle multidimensional sequences (images) we needed to extend the definition of  $\vec{PE}$  to multiple dimensions and heterogeneous inputs (pixel coordinates  $u$  and  $v$  and depth/disparity  $d$ ). We settled on summing

together the embedding of each dimension:

$$\vec{PE}_2(u_n, v_n) = \vec{PE}(u_n) + \vec{PE}(v_n) \quad (2)$$

$$\vec{PE}_3(u_n, v_n, d_n) = \vec{PE}(u_n) + \vec{PE}(v_n) + \vec{PE}(d_n) \quad (3)$$

This implies that all directional encodings contribute equally to the final token representation, avoiding directional biases. A visual representation of the difference between  $\vec{PE}_2$  and  $\vec{PE}_3$  is reported in Fig. 3, where three target pixels (red, green, blue) are sampled from an input image (top row) and the similarity in embedding between them and each other pixel is reported in the bottom two images using the same colors. The image in the bottom left shows similarity scores according to  $\vec{PE}_2$ , while the bottom right the ones according to  $\vec{PE}_3$ . One can easily appreciate the much richer description of the content offered by the three-dimensional encoding, which captures the stronger relation between pixels belonging to the same object. Notice, for example, how the car in the center (blue target pixel) is clearly identifiable in the similarity representation.

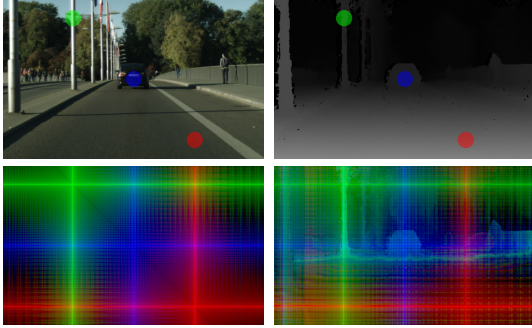


**Fig. 3:** Comparison between 2D (left) and 3D (right) positional encoding. The pixels highlighted in the two top images are used as targets: the distance between them and all other pixels is represented in the bottom images.

### 3.2. Multimodal Attention

For the multimodal setup we exploit a shared-weights parallel branches encoder. The relevant information is shared between the two modalities using two modules: a Cross-Input Attention (CIA) and an Attention-Mix (AM) one. To better describe the CIA block, we report the original formulation of a Transformer self-attention module and show how it can be modified:

$$\text{Attention}(Q, K, V) = \text{softmax}\left(\frac{QK^T}{\sqrt{d_{\text{head}}}}\right)V \quad (4)$$

where  $Q$  is the query,  $K$  is the key,  $V$  is the value and  $d_{\text{head}}$  is the dimension of the head [3]. The attention operation can be thought of as a retrieval process, where a

generic query  $Q$ , specified by a key  $K$  is used to retrieve a value  $V$ . This concept leads to the idea of swapping the self-attention tuples  $(Q, K, V)$  between the color and depth branches in order to allow for retrievals spanning different sources. Given that the key is what specifies the values to be retrieved, it is reasonable to assume that swapping it between modalities provides mutual complementary information to each attention head. This was confirmed by experimental studies, where we observed that swapping the key values led to the best performances. The Cross-Input Attention module can be expressed in mathematical notation as:

$$\begin{aligned} \text{CIA}_c &= \text{Attention}(Q_c, K_d, V_c) \\ \text{CIA}_d &= \text{Attention}(Q_d, K_c, V_d) \end{aligned} \quad (5)$$

where  $c$  and  $d$  represent color and depth (disparity), respectively. In such a manner, the values are re-weighted by the relevance between the queries and the keys of the two different modalities, enhancing features exchange.

Up to this point, the two modalities were processed independently, but they need to be merged before being fed to the SegFormer [4] classifier. Previous research showed that re-aligning multi-resolution outputs between the two modalities would improve consistency [17], therefore we design the Attention-Mix (AM) module with this goal. The module processes each MiT [4] layer output  $O_{[c,d],[1,2,3,4]}$  before it is fed to the segmentation head in the following manner:

$$\begin{aligned} \text{AM}(O_{c,\cdot}, O_{d,\cdot}) &= O_{c,\cdot} \sigma(\text{Conv}(O_{c,\cdot})) + \\ &O_{d,\cdot} (1 - \sigma(\text{Conv}(O_{c,\cdot}))) \end{aligned} \quad (6)$$

Where  $\text{Conv}$  is a  $1 \times 1$  convolution,  $\sigma$  represents the sigmoid function and the multiplication is performed point-wise. A visual representation of this module is reported in the rightmost part of Fig. 1.

## 4. RESULTS

In this section, we present the numerical results attained by our approach on the Cityscapes [6] dataset. We trained our architecture on Cityscapes using the Adam optimizer for 320k iterations on a single RTX 3060 GPU with batch 8, starting from weights pre-trained on ImageNet. The input resolution is  $512 \times 512$ px, and the inference is performed using sliding windows. We follow the learning rate and data augmentation strategies of [4] and set the weight decay rate to 0.01. Per-class IoU results are reported in Table 1 for a color-only baseline, a depth-only baseline, for different configurations of our strategy, and for the transformer-based CMX [8] architecture. From the two baselines, it is possible to see how the exploitation of depth data is more challenging than color information, especially

**Table 1:** Per class IoU results on the Cityscapes [6] dataset, best in **bold**. (r) means that the original code was re-run using our backbone.

| Configuration  | Road | Sidewalk | Building | Wall | Fence | Pole | Traffic Light | Traffic Sign | Vegetation | Terrain | Sky  | Person | Rider | Car  | Truck | Bus  | Train | Motorbike | Bicycle | mIoU |
|----------------|------|----------|----------|------|-------|------|---------------|--------------|------------|---------|------|--------|-------|------|-------|------|-------|-----------|---------|------|
| RGB Baseline   | 97.5 | 83.2     | 90.7     | 47.8 | 56.0  | 44.8 | 56.5          | 67.2         | 91.4       | 68.4    | 94.5 | 78.9   | 49.6  | 93.3 | 68.0  | 71.1 | 73.7  | 57.8      | 70.1    | 71.6 |
| Depth Baseline | 95.7 | 72.8     | 84.0     | 27.9 | 36.4  | 31.4 | 34.0          | 39.1         | 80.0       | 49.2    | 83.3 | 60.4   | 27.3  | 85.1 | 45.9  | 49.8 | 37.5  | 32.9      | 47.7    | 53.7 |
| CMX [8] (r)    | 97.2 | 78.6     | 90.2     | 53.2 | 50.0  | 52.4 | 56.8          | 63.7         | 91.0       | 62.1    | 94.5 | 72.3   | 44.6  | 90.9 | 50.9  | 65.5 | 19.0  | 37.9      | 64.6    | 65.0 |
| RGBD           | 97.5 | 83.3     | 91.2     | 45.9 | 55.6  | 47.8 | 59.8          | 69.2         | 91.4       | 68.4    | 94.6 | 79.4   | 48.5  | 93.4 | 69.2  | 71.1 | 74.8  | 57.6      | 70.1    | 72.0 |
| 3D PE          | 97.5 | 83.3     | 90.9     | 46.2 | 55.7  | 46.1 | 57.5          | 67.7         | 91.4       | 68.5    | 94.7 | 78.6   | 49.7  | 93.3 | 71.3  | 72.8 | 76.7  | 57.7      | 69.7    | 72.1 |
| cross-V        | 97.5 | 83.4     | 91.1     | 44.8 | 55.7  | 47.8 | 59.7          | 69.3         | 91.5       | 68.4    | 94.6 | 79.5   | 48.7  | 93.4 | 69.0  | 71.1 | 73.7  | 57.7      | 70.0    | 71.9 |
| cross-Q        | 97.5 | 83.3     | 91.2     | 45.2 | 57.2  | 48.1 | 60.0          | 69.2         | 91.5       | 67.8    | 94.6 | 79.5   | 49.4  | 93.4 | 69.2  | 71.3 | 75.3  | 57.4      | 70.4    | 72.2 |
| cross-K        | 97.5 | 83.4     | 91.2     | 45.9 | 56.7  | 47.7 | 59.7          | 69.3         | 91.4       | 68.4    | 94.6 | 79.6   | 49.2  | 93.4 | 69.9  | 71.9 | 75.3  | 58.1      | 70.2    | 72.3 |
| attn-mix       | 97.5 | 83.2     | 91.3     | 45.9 | 56.7  | 48.4 | 60.1          | 69.3         | 91.4       | 68.2    | 94.6 | 79.9   | 50.7  | 93.5 | 70.8  | 72.2 | 77.0  | 57.1      | 70.8    | 72.6 |
| Total          | 97.7 | 84.3     | 91.8     | 43.2 | 58.7  | 52.0 | 63.1          | 72.0         | 91.9       | 69.6    | 94.8 | 81.0   | 52.8  | 94.0 | 71.5  | 74.4 | 76.7  | 60.4      | 71.8    | 73.8 |

due to the introduction of noise and artifacts during the depth estimation, which prevents the network from fitting correctly to the data. Nevertheless, a standard two-branch architecture (RGBD) allows improving performance (up to 72.0%), which indicates the potential of using depth data and suggests that the information provided by the two modalities is complementary.

Notice how the proposed positional encoding achieves better performance than the two branches scheme, at the same time avoiding the extra complexity of the second branch (i.e., with the same complexity as the color-only architecture). Furthermore, CMX’s two-stream architecture is not able to reach good performance when a positional encoder is employed.

When one considers the parallel shared-weights configuration (see Fig. 1) it is possible to see how both our contributions improve performances (see the ablation for more details). Still, the best results are achieved by the combination of all the proposed strategies, which allows reaching an accuracy of 73.8%, with a noticeable gain over the color baseline even in the presence of noisy depth data, which makes the segmentation task more challenging. Notice also that the improvement is consistent across all classes: our approach has the highest per-class accuracy on all except one classes (*Wall*). Furthermore, in Table 2 we report some additional comparisons between our approach and competing works with a similar computational cost. It is possible to see how our approach outperforms both convolutional architectures and transformer-based ones of comparable complexity. In particular, VGG16-based schemes achieve the worst results with a gap with respect to our approach of more than 10.0% mIoU. Other multimodal strategies with lightweight backbones (ResNet18, Adapnet) allow for better performances but not enough to reach our approach. Importantly, CMX [8] offers a more direct comparison given that it adapts the same architecture of our approach, SegFormer [4]. It has been tested using the same backbone on the same RGBD data and the outcomes we obtained show that our improvements allow for much better performances.

**Table 2:** Comparison between our approach and competitors with backbones of similar complexity.

| Method       | Backbone    | mIoU |
|--------------|-------------|------|
| CMFNet [17]  | VGG16       | 60.0 |
| MDASS [18]   | VGG16       | 63.1 |
| CMX [8] (r)  | MiT-B0 (PE) | 65.0 |
| RSSAWC [19]  | ICNet       | 65.1 |
| RTFNet [20]  | ResNet18    | 69.4 |
| AdapNet [21] | AdapNet     | 71.7 |
| DepthFormer  | MiT-B0 (PE) | 73.8 |

#### 4.1. Ablation

Finally, we analyze the impact of all components of our approach. Numerical results are reported in Table 1, note that the ablation experiments were trained for 160k iterations for speed/efficiency tradeoffs. For what regards the positional encoding (Sec. 3.1), our approach shows an improvement of 0.5% of mIoU w.r.t. the color baseline, without any increase in the number of architecture parameters or significant computational costs. The cross-input attention (Sec. 3.2) is analyzed through the cross-Q/K/V simulations. Here we can see how the swap of the values leads to small but noticeable performance degradation over the RGBD baseline. This corresponds to a naive approach which swaps attention weights between modalities, since in our shared-weight setting swapping both  $K$  and  $Q$  (i.e., the attention weights) is equivalent to swapping  $V$ . Swapping keys or queries, instead, leads to an improvement over the baseline, reaching a mIoU of 72.3% in the case of keys (that slightly outperform queries). These gains are also justified by reasoning over the operations performed by an attention layer (Sec. 3.2). Finally, the Attention-Mix module shows an improvement of 0.6% in mIoU compared to naive RGBD where the multi-head features are simply summed layer-wise, confirming the necessity of careful feature mixing.

## 5. CONCLUSIONS

In this work we introduced a strategy that efficiently embeds depth information in the positional encoding of a transformer-based segmentation architecture, improving the final accuracy. We have also shown how performing cross-attention by acting at the input level can enhance information sharing between parallel network branches, as hinted by the Query-Key-Value interpretation of an attention layer. These claims were supported by numerical results and ablation studies on the Cityscapes dataset. In the future, we plan to explore different formulations of positional encodings and different input modalities.

## 6. REFERENCES

- [1] Y. Mo, Y. Wu, X. Yang, F. Liu, and Y. Liao, "Review the state-of-the-art technologies of semantic segmentation based on deep learning," *Neurocomputing*, vol. 493, pp. 626–646, 2022.
- [2] A. Dosovitskiy, L. Beyer, A. Kolesnikov, D. Weissenborn, X. Zhai, T. Unterthiner, M. Dehghani, M. Minderer, G. Heigold, S. Gelly *et al.*, "An image is worth 16x16 words: Transformers for image recognition at scale," *arXiv:2010.11929*, 2020.
- [3] A. Vaswani, N. Shazeer, N. Parmar, J. Uszkoreit, L. Jones, A. N. Gomez, Ł. Kaiser, and I. Polosukhin, "Attention is all you need," *NIPS*, vol. 30, 2017.
- [4] E. Xie, W. Wang, Z. Yu, A. Anandkumar, J. M. Alvarez, and P. Luo, "Segformer: Simple and efficient design for semantic segmentation with transformers," *NIPS*, vol. 34, 2021.
- [5] G. Rizzoli, F. Barbato, and P. Zanuttigh, "Multimodal semantic segmentation in autonomous driving: A review of current approaches and future perspectives," *Technologies*, vol. 10, no. 4, 2022.
- [6] M. Cordts, M. Omran, S. Ramos, T. Rehfeld, M. Enzweiler, R. Benenson, U. Franke, S. Roth, and B. Schiele, "The cityscapes dataset for semantic urban scene understanding," in *CVPR*, 2016, pp. 3213–3223.
- [7] A. Valada, R. Mohan, and W. Burgard, "Self-supervised model adaptation for multimodal semantic segmentation," *IJCV*, vol. 128, no. 5, pp. 1239–1285, 2020.
- [8] H. Liu, J. Zhang, K. Yang, X. Hu, and R. Stiefelhagen, "Cmx: Cross-modal fusion for rgb-x semantic segmentation with transformers," *arXiv:2203.04838*, 2022.
- [9] P. Testolina, F. Barbato, U. Michieli, M. Giordani, P. Zanuttigh, and M. Zorzi, "Selma: Semantic large-scale multimodal acquisitions in variable weather, daytime and viewpoints," *arXiv:2204.09788*, 2022.
- [10] C. Couprie, C. Farabet, L. Najman, and Y. Lecun, "Indoor semantic segmentation using depth information," in *ICLR*, 2013, pp. 1–8.
- [11] G. Pagnutti, L. Minto, and P. Zanuttigh, "Segmentation and semantic labelling of rgb-d data with convolutional neural networks and surface fitting," *IET Computer Vision*, vol. 11, no. 8, pp. 633–642, 2017.
- [12] Q. Zhang, S. Zhao, Y. Luo, D. Zhang, N. Huang, and J. Han, "Abmdrnet: Adaptive-weighted bi-directional modality difference reduction network for rgb-t semantic segmentation," in *CVPR*, June 2021, pp. 2633–2642.
- [13] G. Krispel, M. Opitz, G. Waltner, H. Possegger, and H. Bischof, "Fuseseg: Lidar point cloud segmentation fusing multi-modal data," in *WACV*. arXiv, 2020, pp. 1874–1883.
- [14] X. Chen, K.-Y. Lin, J. Wang, W. Wu, C. Qian, H. Li, and G. Zeng, "Bi-directional cross-modality feature propagation with separation-and-aggregation gate for rgb-d semantic segmentation," in *ECCV*. Springer, 2020, pp. 561–577.
- [15] D. Seichter, M. Köhler, B. Lewandowski, T. Wengefeld, and H.-M. Gross, "Efficient rgb-d semantic segmentation for indoor scene analysis," in *ICRA*. IEEE, 2021, pp. 13 525–13 531.
- [16] W. Wang, E. Xie, X. Li, D.-P. Fan, K. Song, D. Liang, T. Lu, P. Luo, and L. Shao, "Pyramid vision transformer: A versatile backbone for dense prediction without convolutions," in *ICCV*, 2021, pp. 568–578.
- [17] Y. Zhang, O. Morel, R. Seulin, F. Mériaudeau, and D. Sidibé, "A central multimodal fusion framework for outdoor scene image segmentation," *Multimedia Tools and Applications*, vol. 81, no. 9, pp. 12 047–12 060, 2022.
- [18] H. Rashed, A. El Sallab, S. Yogamani, and M. El-Helw, "Motion and depth augmented semantic segmentation for autonomous navigation," in *CVPRW*, 2019, pp. 0–0.
- [19] A. Pfeuffer and K. Dietmayer, "Robust semantic segmentation in adverse weather conditions by means of sensor data fusion," in *Int. Conf. on Information Fusion (FUSION)*. IEEE, 2019, pp. 1–8.
- [20] Y. Sun, W. Zuo, and M. Liu, "Rtfnnet: Rgb-thermal fusion network for semantic segmentation of urban scenes," *IEEE RAL*, vol. 4, no. 3, pp. 2576–2583, 2019.
- [21] A. Valada, J. Vertens, A. Dhall, and W. Burgard, "Adapnet: Adaptive semantic segmentation in adverse environmental conditions," in *ICRA*. IEEE, 2017, pp. 4644–4651.